Structural Chemistry
https://doi.org/10.1007/s11224-020-01646-1

ORIGINAL RESEARCH

The adsorption of bromochlorodifluoromethane on pristine and Ge-doped silicon carbide nanotube: a PBC-DFT, NBO, and QTAIM study

Mohsen Doust Mohammadi[1] · Hewa Y. Abdullah[2]

Received: 22 July 2020 / Accepted: 16 September 2020

Abstract
In the present investigation, the feasibility of detecting the bromochlorodifluoromethane (BCF) gas molecule onto the outer surface of pristine single-wall silicon carbide nanotube (SiCNT), as well as its germanium-doped structures (SiCGeNT), was carefully evaluated. For achieving this goal, a density functional theory level of study using the Perdew, Burke, and Ernzerhof exchange-correlation (PBEPBE) functional together with a 6-311G(d) basis set has been used. Subsequently, the B3LYP, CAM-B3LYP, ωB97XD, and M06-2X functionals with a 6-311G(d) basis set were also employed to consider the single-point energies. Natural bond orbital (NBO) and quantum theory of atoms in molecules (QTAIM) were implemented by using the PBEPBE/6-311G(d) method, and the results were compatible with the electronic properties. In this regard, the total density of states (TDOSs), the Wiberg bond index (WBI), natural charge, natural electron configuration, donor-acceptor natural bond orbital interactions, and the second-order perturbation energies are performed to explore the nature of the intermolecular interactions. All of the energy calculations and population analyses denote that by adsorping of the gas molecule onto the surface of the considered nanostructures, the intermolecular interactions are of the type of strong physical adsorption. The doped nanotubes have a very high adsorption energy compared with pristine nanotube. Generally, it was revealed that the sensitivity of the adsorption will be increased when the gas molecule interacts with decorated nanotubes and decrease the HOMO-LUMO band gap; therefore, the change of electronic properties can be used to design suitable nanosensors to detect BCF gas.

Keywords Bromochlorodifluoromethane · BCF · Silicon carbide · Nanotube · Density functional theory · Freon 12B1 · Natural bond orbital

Introduction

The nanomaterials are structurally divided into carbon and non-carbon materials. Carbon nanotube (CNT), which is an allotrope of carbon, was first discovered independently by Iijima et al. [1] and Bethune et al. [2] in 1991 in soot from carbon discharge in a neon-containing medium [3–7]. The CNT, according to its (n,m) type, presents stupendous mechanical [8–10], electromagnetic [11–15], and chemical [16–19] properties, and it plays a significant role in various branches of technology. One of the most applicable binary carbide-derived carbons of CNT with extensive properties is silicon carbide nanotube (SiCNT) [20]. There have also been widespread reports on the applications of SiCNT as active material in electrodes [21, 22], gas storage materials [23, 24], and catalysts [25–27].

In the last two decades, theoretical studies in the density functional theory (DFT) framework on nanostructures have attracted the attention of many scientists in the fields of computational chemistry and solid-state physics [28–32]. The study of silicon carbide nanotube is no exception, and many theoretical studies on this nanostructure have led to interesting proposals for the manufacture of the industrial devices. Theoretical studies show the

✉ Hewa Y. Abdullah
hewayaseen@gmail.com

[1] School of Chemistry, College of Science, University of Tehran, Tehran 14176, Iran

[2] Physics Education Department, Faculty of Education, Tishk International University, Erbil 44001, Iraq

Published online: 22 September 2020

molecular stability, structure, and properties of SiCNT [33, 34]. In this regard, Alam et al. proved that the most stable form of SiCNT is the arrangement in which the Si atom is surrounded by three carbon atoms [35]. Compared with the CNT, the SiC nanotube shows high thermal stability as well as a larger HOMO-LUMO gap (HLG) [36]. Ahmadi et al. show that by dopping the gallium element to the SiCNT, the semiconductor properties will be improved [37]. Having a wide surface, SiCNT can appear in the role of an adsorbent and be used in the design of relevant tools. Mohammadi et al. have had a precise investigation on the adsorption of noble gases and bromomethane onto the SiCNT [28, 31]. A biotechnology study by Chen et al. introduced (8,0) SiCNT for encapsulation of the glycine molecule [38]. Several toxic gases can be trapped using SiCNT such as CO [39], NO [40], N_2O [41], and CO_2 [42]. The widespread use of silicon carbide nanotubes provides the basis for further study on such structures.

Bromochlorodifluoromethane (BCF) (also is known as Freon 12B1or Halon-1211 with chemical formula ($CBrClF_2$) is classified as a category 2 carcinogen from the group of chlorofluorocarbons or dihalomethanes. It is a colorless, odorless, flammable gas with a solid monoclinic crystal structure of space group P21 [43]. Bromochlorodifluoromethane was used as the refrigerant. It is listed in the Montreal Protocol as a substance that degrades the ozone layer [44]. A rotational study has been performed by Caminati et al. [45] to investigate the dimer interactions of BCF molecule, and the results confirm that the interactions are non-covalent. According to the dissociation energy of dimer complex of CMF molecule reported in [45], we considered it as an isolated single molecule in this work.

This article discusses the design of such a sensor. This study investigated the interactions of BCF with SiCNT and SiCGeNT. After optimizing the structure of silicon carbide nanotubes by Gaussian software, to study the chemical stability and conductivity, the elements doping process on this nanotube have been studied. Because of the high sensitivity of computation to precisely determine the energy of molecular orbitals to investigate the conductivity and probability of physical and chemical adsorption, different structures need to be optimized using appropriate computational methods. For this purpose, the PBEPBE functional and 6-311G(d) basis set were used in this research for computation. The B3LYP, CAM-B3LYP, ωB97XD, and M06-2X functionals with 6-311G (d) basis set were also used to calculate the single-point energies. Natural bond orbital and quantum theory of atoms in molecules were studied by using the PBEPBE/6-311G (d) method, and the results were used to obtain various physical parameters.

Computational details

The DFT calculations at Perdew, Burke, and Ernzerhof (PBEPBE) functional [46] together with 6-311G(d) Pople split-valence triple-zeta basis set with polarization functions [47] were used for geometry optimization for all different positions of the BCF/tube complex structures. To determine the stability of the optimized structures, frequency calculations are also performed using the similar level of theory to approve that all the stationary points are in agreement with a minimum point through the potential energy surface. For further investigation, single-point energy calculations using different levels of theory were also applied on the most stable relaxed structures, which were obtained from geometry optimization at the PBEPBE/6-311G(d) level. The levels of theory used for the single-point energy calculations included B3LYP, CAM-B3LYP, M06-2X, and ωB97XD together with 6-311G(d) basis set. Natural bond orbital (NBO) and quantum theory of atoms in molecules (QTAIM) were implemented by using the PBEPBE/6-311G(d) method. All of the calculations including geometry optimization, single-point energy calculations, and NBO analysis were performed by Gaussian 16 package [48]. It should be noted that the NBO calculations were performed using the NBO v 3.0 software which is embedded within Gaussian software. In order to perform quantum theory of atoms in molecule (QTAIM) and density of state (DOS) analyses, the Multiwfn program [49–51] was employed.

The adsorption energy (E_{ads}) of the investigated BCF onto the surface of pristine and doped nanotubes can be calculated as follows:

$$E_{ads} = E_{sheet/CFM} - (E_{sheet} + E_{CFM}) \quad (1)$$

where $E_{tube/BCF}$ represents the total energy of the complex structure. E_{tube} and E_{BCF} are the total energy of the pure nanotube and the pure BCF molecule, respectively. It is noteworthy that the absorption energy consists of two parts: the interaction energy (E_{int}) and the deformation energy (E_{def}) that occur in the absorption process. Therefore, the following equations are used to calculate these shares:

$$E_{ads} = E_{int} + E_{def} \quad (2)$$

$$E_{int} = E_{sheet/CFM} - E_{sheetincomplex} - E_{CFMincomplex} \quad (3)$$

$$E_{def} = E_{def}^{sheet} + E_{def}^{CFM} = \left(E_{sheetincomplex} - E_{pristinesheet}\right) + \left(E_{CFMincomplex} = E_{isolatedCFM}\right) \quad (4)$$

where $E_{sheet\ in\ complex}$ and $E_{CFM\ in\ complex}$ are energies of BCF molecule and nanotube in the optimized complexes, respectively.

Result and discussion

The structural analysis

To optimize the structure of pristine armchair (5,5) single-walled silicon carbide nanotubes using periodic boundary condition density functional theory (PBC-DFT) [52–55], we first consider a unit cell of silicon and carbon atoms ($Si_{20}C_{20}$) which is 6.274 Å in length. Unlike the nanosheet, the nanotube is expanded in one direction only. We optimized this cell by 1D PBC-DFT method with PBEPBE functional together with basis set 6-311G (d). After optimization of the pristine unite cell, we substituted Ge atom with Si atom then the optimization process has been repeated for doped nanotubes. The quantitative values of bond lengths are shown in Fig. 1.

The next step was the optimization of BCF/nanotube complexes. In this step, the BCF molecule was placed on the outer surface of each abovementioned nanotubes with vertical distance of about 2.1 Å. To find out the optimum distances between nanotube and BCF molecule, we used the rigid scan for some cases to estimate the most efficient distance. It should be noted that the level of theory in both optimization and rigid scan was PBEPBE/6-311G (d). To better explain the details of the adsorption process, it will be useful to compare Figs. 1 and 2.

The silicon carbide nanotube is composed of several symmetric hexagons that have four different adsorption positions for the adsorption of any molecule onto the outer surface of the nanotube as shown in Fig. 3: adsorption position on Si atom (T_1); adsorption position on C atom (T_2); and adsorption position on SiC bond (T_3); adsorption position at hexagonal center (T_4). The logical approach is to put the BCF molecule in each of these positions and measure the amount of adsorption energy (E_{ads}). It is important to note that the BCF molecule has different heads (Br, Cl, F), and each of these heads must be placed on the desired position on the nanotube to measure the amount of absorption energy. Our experience shows that negligible differences exist in the amounts of adsorption energies when we place the BCF in any of the possible adsorption sites. As mentioned in [56], when the differences in the adsorption energies are "below the range of chemical interest," placing the gas in different positions on the nanotubes provides identical results. Nevertheless, we put the BCF molecule from Br-head onto the desired positions on the SiC nanotube. The test result showed that there is a negligible difference among the adsorption energies; therefore, the Si atom position was the target position on the SiC nanotube.

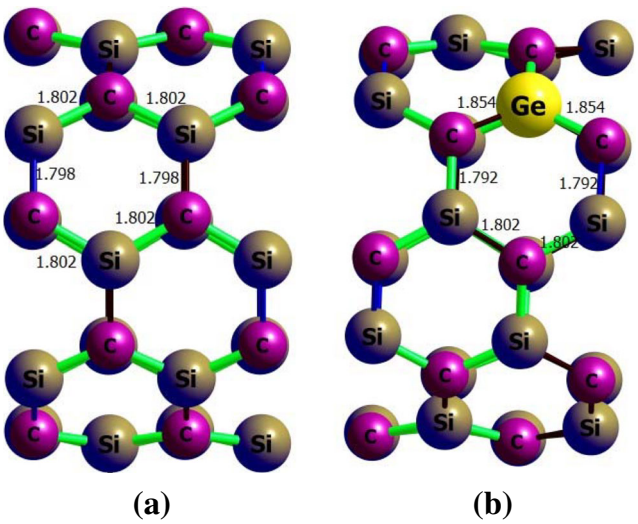

Fig. 1 The values of bond length for (**a**) SiCNT and (**b**) SiCGeNT. The optimization process has been done using PBEPBE/6-311G (d) level of theory

Next, we extend the unit cell to five units and terminated with hydrogen atoms (Fig. 4); the nanotube length for $Si_{100}C_{100}H_{20}$ increased to 31.804 Å, then single-point energy calculations using different functional such as PBEPBE, ωB97XD, and M06-2X and 6-311G (d) basis set were done. The calculated values indicate a strong interactions between nanotubes and BCF molecule. Since the PBEPBE functional does not account for the long-range scattering contribution, it is expected that in poor interactions, this functional will not give a good estimate of the amount of energy. For this reason, methods have been developed for long-range and dispersion effects. In this work, we used PBEPBE and ωB97XD to consider long-range and dispersion effects. The well-known M06-2X functional is used to better comparison. The results show that the energies obtained from the PBEPBE and other functionals are consistent with the accuracy of the calculations. On the other hand, as expected, the ωB97XD method shows more energy values than the others, due to the dispersion contribution consideration. Also, by doping the Ge element on the SiC nanotube, significant changes in the results are achieved. Table 1 shows that Ge doping increase the absorption energy and enhanced the chemical absorption. Table 2 also shows the bond length and the nearest intermolecular distances (re (Å)) between BCF molecule and SICNT and SiCGeNT.

Energetics properties

The chemical electron potential (μ) describes the tendency of electrons to escape from a particular species at the ground state. This quantity is equal to the absolute negative electronegativity obtained from the definition provided by Mulliken, as follows:

$$\mu = -\chi_M \tag{5}$$

Parr and his colleagues [57] used the DFT to show that at a constant external potential, the potential energy of an electron

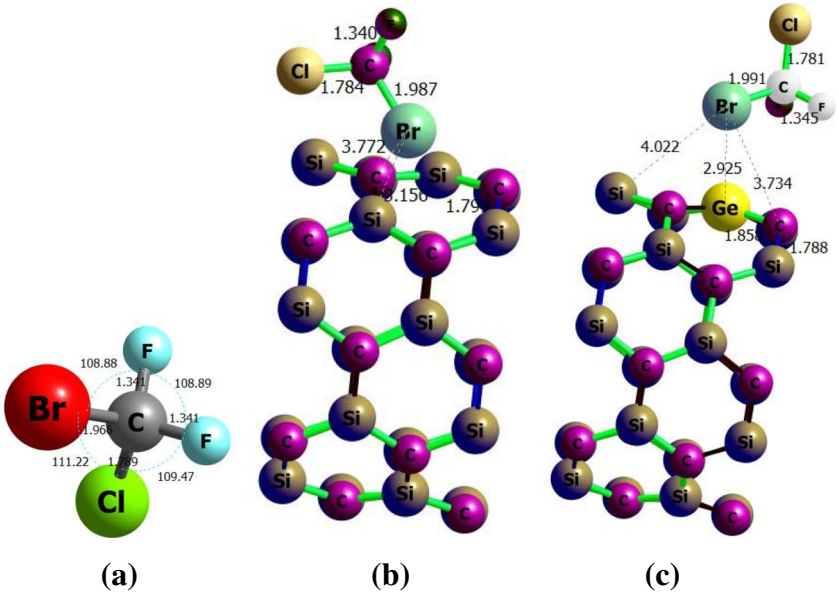

Fig. 2 The most stable form of (**a**) isolated BCF and the adsorbed BCF molecule onto the outer surface of (**b**) SiCNT and (**c**) SiCGeNT. All clusters have been optimized using the PBEPBE functional and 6-311G(d) basis set

is related to the first derivative of energy relative to the number of electrons, as follows:

$$\mu = \left(\frac{\partial E}{\partial N}\right)_{\upsilon(r)} = -\frac{1}{2}(IP + EA) \tag{6}$$

where *IP* and *EA* are the ionization affinity and electron affinity, respectively [58]. Based on the Koopman approximation (see the Hartree–Fock theory) and Janak's approximation [59]

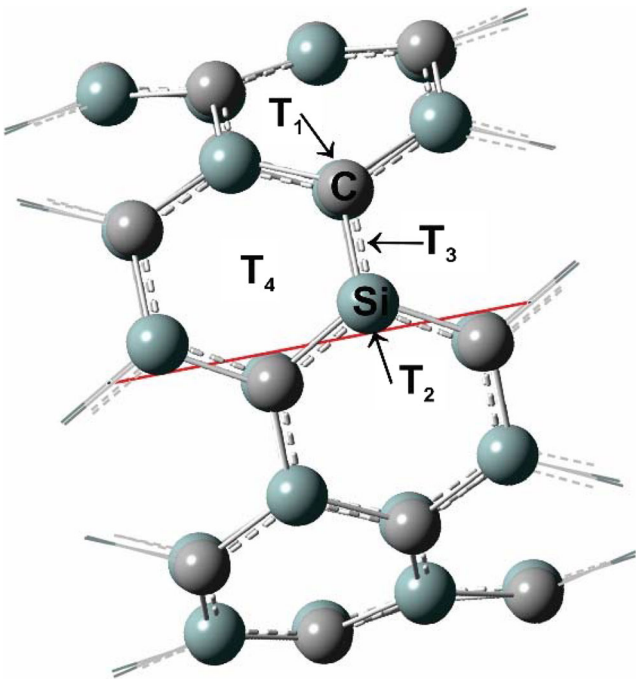

Fig. 3 All possible target positions for the adsorption of any arbitrary molecules onto the surface of SICNT. Top of boron atom (T_1), top of nitrogen atom (T_2), between boron and nitrogen atoms (T_3), and top of the hexagonal ring (T_4)

(in the DFT theory), the ionization and electron affinity potentials are equal to the negative value of the highest occupied molecular orbital (HOMO) energy ($\varepsilon_{HOMO} = -IP$) and negative value of the lowest unoccupied molecular orbital (LUMO) ($\varepsilon_{LUMO} = -EA$). Therefore, the chemical potential in Janak's approximation is defined as:

$$\mu = \left(\frac{\partial E}{\partial N}\right)_{\upsilon(\vec{r})} \cong \frac{(\varepsilon_{LUMO} + \varepsilon_{HOMO})}{2} \tag{7}$$

where ε_{HOMO} and ε_{LUMO} are the energies of the HOMO and the LUMO, respectively. N is the number of electrons, E is the total electronic energy of the system, and $\upsilon(r)$ is the external potential.

Comparison of the variation in electron chemical potentials to that in the number of electrons at a constant external potential is called chemical hardness, which is expressed as:

$$\eta = \left(\frac{\partial \mu}{\partial N}\right) = \frac{1}{2}\left(\frac{\partial^2 E}{\partial^N}\right) \tag{8}$$

Parr et al. [60]] used the electron energy curve as well as the finite difference approximation to express hardness as follows:

$$\eta = \frac{1}{2}(IP{-}EA) \tag{9}$$

Moreover, using Janak and Koopman's approximations, the hardness equation is transformed as follows:

$$\Delta E_{\min} = -\frac{\mu^2}{2\eta} \tag{10}$$

Chemical hardness is the energy gap between the HOMO and the LUMO. Therefore, molecules with high energies are

Table 1 The adsorption energy (E_{ads}) for SiCNT and SiCGeNT with BCF molecule. All values are in (eV)

System	PBEPBE	B3LYP	CAM-B3LYP	M06-2X	ωB97XD
$CBrClF_2$_SiCNT	− 2.063	− 1.286	− 1.697	− 2.687	− 2.960
$CBrClF_2$_SiCGeNT	− 3.462	− 2.562	− 3.009	− 3.930	− 4.160

considered as hard molecules, while those with low energies are called soft molecules. Since the softness of a molecule is the opposite of its hardness, the equation for molecule softness is denoted as follows [61]:

$$S = \frac{1}{\eta} \tag{11}$$

Inspired by Maynard's work, Parr et al. [62] introduced electrophilicity as the steady-state energy in which an atom or a molecule at ground state gains by receiving additional electron charges from the environment. The energy changes that lead to such a charge transfer are expressed as follows:

$$\Delta E = \mu \Delta N + \frac{1}{2}\eta(\Delta N)^2 \tag{12}$$

When the system receives electron charges from the environment sufficient to equate its potential to that of the environment, the system is saturated with electrons and can be expressed as follows:

$$\frac{d\Delta E}{d\Delta N} = 0 \tag{13}$$

The electron load received from the environment is maximized, and the total energy of the system is eventually minimized. Thus:

$$\Delta N_{\max} = -\frac{\mu}{\eta} \tag{14}$$

$$\Delta E_{\min} = -\frac{\mu^2}{2\eta} \tag{15}$$

Since $\eta > 0$, $\Delta E < 0$ always, and the charge transfer is energetically desirable. Accordingly, Parr et al. proposed the following equation to denote the electrophilicity of electrophilic species.

$$\omega = \frac{\mu^2}{2\eta} \tag{16}$$

In fact, the electrophilicity index is the capacity of a species to accept an arbitrary number of electrons from the environment. In this regard, Nourizadeh and Maihami [63] used electrophilicity in the Diels–Alder reaction and stated that "atoms appear to be arranged in a natural tendency to reach the lowest electrophilicity." This expression is called the minimum electrophilicity principle (MEP).

The values of maximum occupied molecular orbital (HOMO) and lowest occupied atomic orbital (LUMO), and their differences (HLG), chemical potential (μ), chemical hardness (η), and electrophilicity (ω) are reported in Table 3. From the results of this table, it can be seen that by adsorption of BCF molecule onto the outer surface of nanotubes, the distance between HOMO and LUMO levels is reduced relative to the pure nanotube, which is caused by the molecular energy absorption matched from this position. By doping the elements Al and Ga, it is observed that HLG changed. The decrease in HLG results in an increase in the electrical conductivity and thus an increase in the metal property of all the nanotubes compared with pure SiCNT. It is also noteworthy that the observed changes in HLG after doped Ge is mainly due to lower LUMO energy levels. In order to study these changes in the electron structure of the studied cases more closely, the density of state spectra (DOS) will be analyzed

Table 2 The bond lengths and the nearest intermolecular distances (re (Å)) between BCF molecule and SiCNT and SiCGeNT. All calculations were performed using PBC-DFT PBEPBE/6-311G(d) level of theory. The dashed line (....) shows the intermolecular interactions between atoms of BCF and nanotube, and the em dash (—) shows the bonds between atoms in one molecule

Systems	Br....Ge	Br....C	Br....Si	C—Ge	Si—C	C—Br	C—Cl	C—F
$CBrClF_2$	-	-	-	-	-	1.966	1.789	1.341
SiCNT	-	-	-	-	1.800	-	-	-
SiCGeNT	-	-	-	1.854	1.792	-	-	-
$CBrClF_2$/SiCNT	-	3.772	3.156	-	1.799	1.987	1.784	1.340
$CBrClF_2$/SiCGeNT	2.925	3.734	4.022	1.858	1.788	1.991	1.781	1.345

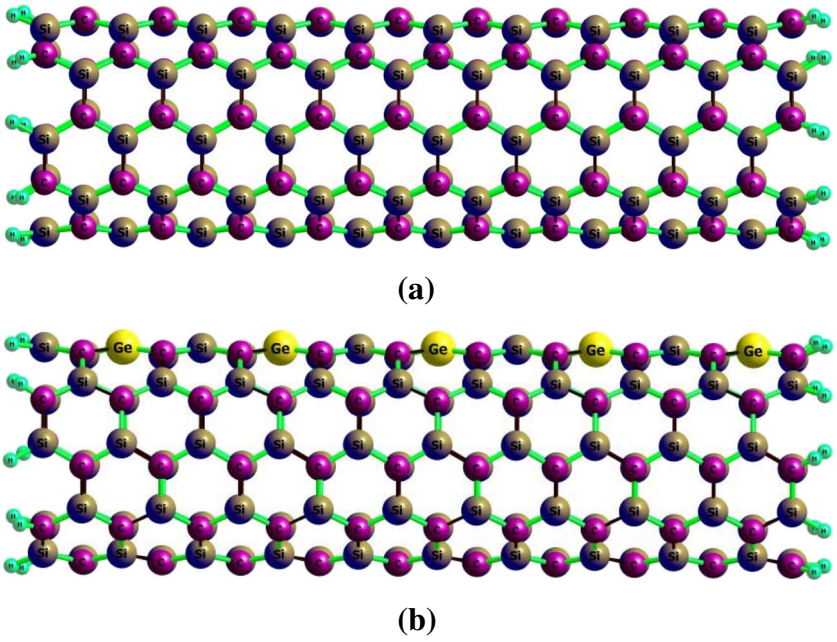

Fig. 4 The expanded (**a**) silicon carbide and (**b**) Ge-doped silicon carbide nanotubes terminated with hydrogen atoms

in the next section. For a more detailed study of the electron structure changes, the density of state spectra (DOS) are extracted and illustrated in Fig. 5.

From the DOS spectra, it is clear that DOS spectra for all absorption are in agreement with the values of the energy parameters reported in Table 3. The lowest amount of adsorption energy is related to the pristine nanotube, and the highest amount of adsorption energy is for the adsorption of BCF onto the Ge-doped SiC nanotube; the most changes are also observed in the DOS spectrum relative to this nanotube. In other words, the electron structure changes show a direct relationship with the absorption energies. Given the amount of absorption energy, high amount of binding energy, and the structure of DOS spectra obtained in all of these cases, it can be claimed that the adsorption of BCF molecule onto SiC and SiCGe nanotubes is a strong physical adsorption type.

Table 3 Values of HOMO energy (ε_H), LUMO energy (ε_L), HOMO and LUMO energy gap (HLG), chemical potential (μ), chemical hardness (η), and electrophilicity (ω). All values are in (eV) and were obtained from completed nanotube PBEPBE/6-311G (d) level of theory

Systems	ε_H	ε_L	HLG	μ	η	ω
SiCNT	−4.818	−2.723	2.095	−3.770	1.048	7.447
SiCGeNT	−4.805	−2.735	2.070	−3.770	1.035	7.355
$CBrClF_2$/SiCNT	−4.746	−2.789	1.957	−3.768	0.978	6.944
$CBrClF_2$/SiCGeNT	−4.679	−2.964	1.715	−3.821	0.858	6.262

NBO analysis

The natural bond orbital (NBO) analysis has been developed based on many-electron molecular wave function in terms of localized electron-pair bonding units and uses first-order reduced density matrix of the wave function [64, 65]. In the NBO approach, a given wave function should be transformed into a localized form in which NBO are considered as local block eigenfunctions of the density matrix. NBO analysis is applicable in both closed-shell and open-shell systems which are calculated from atom-centered basis functions [66]. The mechanism of the energetic analysis of NBO interactions is based on the one-electron effective energy operator (Fock or Kohn-Sham matrix) that arises from the host electronic structure system (ESS). Second-order perturbation theory is one of the highest used methods for estimating energy effects. For the case of HF or DFT methods, the interactions between NBOs are considered to analyze the wave function energetically, with the explanation that the Kohn-Sham matrix elements are implemented in the DFT platform [67–77].

We used the PBEPBE/6-311g(d) level of theory to perform the NBO calculations. The concept of bonded orbitals can be used to understand the distribution of electrons in atomic and molecular orbitals. Atomic charges and molecular bonds can be used to obtain these orbitals. In this method, an electron density matrix is used to both define the shapes of the atomic orbitals in the molecular environment and obtain molecular bonds (electron density between atoms). NBO is defined as the following equation for σ bonding between atoms A and B.

$$\sigma_{AB} = C_A h_A + C_B h_B \tag{18}$$

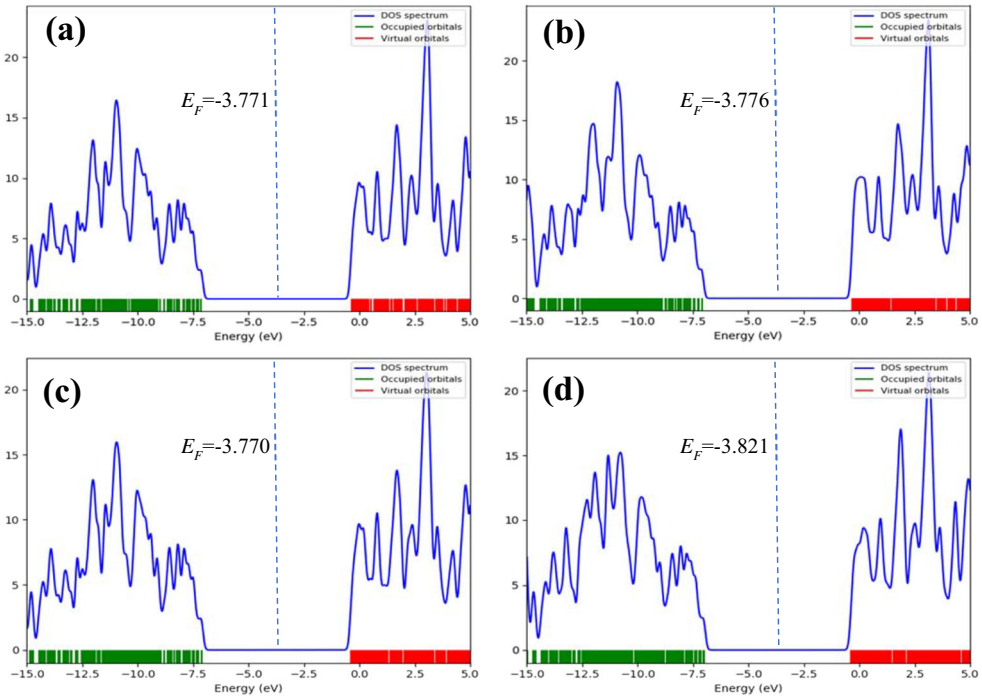

Fig. 5 The density of state (DOS) diagrams for the (**a**) SiCNT, (**b**) BCF/SiCNT, (**c**) SiCGeNT, and (**d**) BCF/SiCGeNT. The data were obtained from completed nanotube and PBEPBE/6-311G (d) level of theory. The values of Fermi energy (E_F) are shown using dashed line

where h_A and h_B are natural hybrids on the A and B atoms. In the covalent limit, $C_A = C_B$, and at the ionic limit, $C_A >> C_B$ (if the electronegativity of A is greater than B). Each bonding NBO must be paired with a corresponding anti-bonding NBO.

$$\sigma^*_{AB} = C_A h_A - C_B h_B \tag{19}$$

Binding orbital analysis is used to evaluate the effects of non-stationary effects, such as anomeric effect, rotation barrier, and hydrogen bonding. In NBO analysis, molecular energy is divided into two parts: total energy (for non-stationary enters) and Lewis molecule energy (where super-conjugation does not occur, and the electrons are strongly bound in single bonds and pairs). The occupied NBO describe the covalent effects in the molecule, while the non-occupied NBO are used to describe non-covalent effects. The most important non-occupied NBO are anti-bond orbitals [64, 76, 77].

Various types of bond order analyses are developed to take into account the bond property such as Mulliken bond order analysis [78], Mayer bond order analysis [79, 80], multi-center bond order analysis [81, 82], Wiberg bond order analysis [83], and fuzzy bond order [84, 85]. Due to the different assumptions, caution should be exercised when using the abovementioned methods, and the term "Caveat emptor" in this case is a practical example to describe such a situation. Basis set containing diffuse functions as case in point leads to unreliable result for Mulliken or Mayer analyses [49]. According to the literature [86], the Wiberg bond order, in comparison with the Mayer method, has much less sensitivity to the basis set. The Wiberg bond index (WBI) is the sum of squares of off-diagonal density matrix elements between atoms and is denoted as follows:

$$\mathrm{WBI} = \sum_k P^2_{jk} = 2P_{jj} - P^2_{jk} \tag{20}$$

where *Pjk* represents the density matrix elements (i.e., the contribution of interactions between basis functions j and k), and *Pjj* is the charge density in the atomic orbital. In the WBI, there is no difference between net bonding or anti-bonding type of elements of the density matrix.

NBO analysis was used to calculate the bond order using the Wiberg method [83] for a more detailed examination of the types of interactions. After studying the adsorption energy of the complexes, we examine the bond length and bond order of the gases and the nanotubes before and after the adsorption. The Wiberg bond order for these clusters is reported in Table 4. According to this table, the bond of the halogen atoms in BCF molecules oriented to the Si in SiCNT and Ge in SiCGeNT. The results of the WBI analysis agree with the adsorption energies reported in Table 1. They reveal that these nanotubes show a strong interaction with the gas molecules and can be considered a suitable sensor for such gases.

One of the results of the natural population analysis obtained from NBO calculation is a natural electron configuration which shows the effective valence electron configuration for any atoms in the studied structure. The results of the NBO calculations shed light on the natural electron configuration and partial natural charge, which are useful in the study of the character of the bond between the BCF and the nanotubes.

Table 4 The Wiberg bond index (WBI) obtained for atomic bonds and intermolecular interactions between BCF molecule and SiCNT and SiCGeNT. All calculations were performed using PBEPBE/6-311G(d) level of theory

Systems	Br....Ge	Br....C	Br....Si	C—Ge	Si—C	C—Br	C—Cl	C—F
$CBrClF_2$	-	-	-	-	-	0.986	1.031	0.923
SiCNT	-	-	-	-	0.968	-	-	-
SiCGeNT	-	-	-	0.936	0.974	-	-	-
$CBrClF_2$/SiCNT	-	0.021	0.120	-	0.968	0.936	1.036	0.927
$CBrClF_2$/SiCGeNT	0.191	0.029	0.009	0.876	0.970	0.926	1.045	0.934

The NBO approach was implemented for all atoms in the pristine and cluster systems to reveal the quantities listed in Table 5. Charge transfer quantity between BCF molecule and nanotubes can also be a criteria to study the interaction of nanotube and BCF, such that the stronger the interaction the more the charge transfer between BCF and the nanotube. Table 5 shows that there is a significant charge transfer between two species during adsorption process that would happen.

In addition, by implementing the natural electron configuration, the type of the interaction between nanotubes and BCF molecule will be described. From Table 5, it can be obvious that valance configuration of isolated BCF molecule and nanotubes as well as valance configuration of nanotube/BCF clusters have been increased. Therefore, the interaction of BCF with all nanotubes can be classified as a strong physical adsorption process.

The second-order perturbative is an estimation of donor-acceptor interactions in the NBO basis. NBO analysis expresses the complex quantum-mechanical wave function into a more palpable Lewis-dot-like formalism. Lewis-type NBO are called filled or "donor" orbitals (σ), and non-Lewis-type NBO are called vacant or "acceptor" orbitals (σ^*). For each donor NBO (i) and acceptor NBO (j), the stabilization energy $E(2)$ is calculated as follows [74]:

$$E(2) = \Delta E_{ij}^2 = -q_i \frac{\left(F_{i,j}\right)^2}{\left(\varepsilon_j - \varepsilon_i\right)} \tag{21}$$

where εi and εj are diagonal elements which show the orbital energies, q_i denotes the donor orbital occupancy ($q = 2$ for closed-shell systems and $q = 1$ for open-shell systems), and the off-diagonal NBO Fock matrix element is demonstrated by $F(i,j)$, and ΔE_{ij}^2 is the stabilization energy.

Table 5 Natural electron configurations and natural charges (esu) for the isolated BCF, pristine, and Ge-doped SiCNT nanotubes and their complex structures. All values calculated by the PBEPBE/6-311G(d) level of theory

Systems	atom	Natural charge	Natural electron configuration
SiCNT	Si	1.87	[core]3S(0.70)3p(1.41)3d(0.03)
	C	−1.87	[core]2S(1.35)2p(4.51)
SiCGeNT	Si	1.87	[core]3S(0.70)3p(1.41)3d(0.03)
	C	−1.87	[core]2S(1.35)2p(4.51)
	Ge	1.72	[core]4S(0.86)4p(1.42)4d(0.01)
$CBClF_2$/SiCNT	Si	1.87	[core]3S(0.70)3p(1.41)3d(0.03)
	C	−1.87	[core]2S(1.35)2p(4.52)
	Br	0.10	[core]4S(1.89)4p(4.99)4d(0.01)5p(0.01)
	Cl	0.02	[core]3S(1.87)3p(5.09)3d(0.01)4p(0.01)
	F	−0.29	[core]2S(1.84)2p(5.45)3d(0.01)
	C	0.55	[core]2S(0.99)2p(2.38)3S(0.01)3p(0.05)3d(0.02)
$CBrClF_2$/SiCGeNT	Si	1.87	[core]3S(0.69)3p(1.41)3d(0.03)
	C	−1.87	[core]2S(1.35)2p(4.52)
	Ge	1.68	[core]4S(0.87)4p(1.44)4d(0.01)5p(0.01)
	Br	0.14	[core]4S(1.89)4p(4.95)4d(0.01)5p(0.01)
	Cl	0.03	[core]3S(1.86)3p(5.09)3d(0.01)4p(0.01)
	F	−0.28	[core]2S(1.84)2p(5.45)3d(0.01)
	C	0.55	[core]2S(1.00)2p(2.38)3S(0.01)3p(0.05)3d(0.02)

Table 6 The donor-acceptor NBO interactions and second-order perturbation energies ($E(2)$) for the BCF clusters with SiCNT and SiCGeNT. All values obtained from completed nanotubes at the PBEPBE/6-311G (d) level of theory

Systems	Donor NBO (i)	Acceptor NBO (j)	E2 (kcal/mol)
$CBrClF_2$/SiCNT	BD (Si—C)	RY*(Br)	0.14
	BD (Ge—C)	RY*(Br)	0.44
	BD (Si—C)	BD*(C—F)	0.06
	BD (Si—C)	BD*(C—Cl)	0.05
	BD (Ge—C)	BD*(C—Br)	0.81
$CBrClF_2$/SiCGeNT	BD (Si—C)	BD*(C—Br)	1.01
	BD (Si—C)	RY*(Br)	0.15

The results of electron donor-acceptor electron configuration of pristine SiCNT and Ge-doped SiCNT are reported in Table 6. It is noteworthy that in this table, the most important interactions in terms of the electron transfer stability energy are reported. The existence of such interactions with the remarkable stability energies in this table shows that the doped atom has been incorporated into the nanotube structure by the chemical interaction, and the stability structure has been achieved. In other words, the inserted atom behaves as a doping atom. The data in Table 6 show that the most important interaction for the pristine nanotube related to electron transfer from the BD (Si—C) bond as the electron donor to the BD*(C—Br) as the receptor. This is in agreement with the results of the absorption energy as well as with the other results which have been examined. In the study of the doped complex, it is observed that the Ge electron pair is a donor (Lewis base) and the Br-bonded electron pair is the group of the electron-acceptor molecule (Lewis acid). The highest electron-acceptor stabilization energy in all cases is due to the same interaction, which indicates a strong adsorption of the molecule onto the SiCGe nanotube compared with the pristine NT.

QTAIM analysis

QTAIM is a powerful tool for topology analysis containing the type and structure of bonds and intermolecular interactions. QTAIM method is proposed by Bader et al. [87–92]. According to this theory, the critical point of the electron density, which can be a minimum point, a maximum point, or a saddle point, can fall into one of the following four categories: (1) atomic critical point (ACP), which denotes the geometrical position of an atom or nucleus (other than hydrogen), and geometrically represents a local maximum point of electron density in all three directions of space; (2) bond critical point (BCP), which indicates a critical point related to a bond or physical or chemical interaction (in reality, this point represents a saddle point with two directions of maximum electron density and one direction of minimum electron density); (3) ring critical point (RCP) [93, 94], which denotes a ring or set of atoms forming a ring (geometrically, it is a saddle point with the minimum electron density in one direction and in the other two directions); and (4) cage critical point (CCP), which is observed when multiple rings form a cage (geometrically, this point is a local minimum point in all three directions of space). Poincaré–Hopf relationship should be satisfied to verify if all CP may have been found as follows [95, 96]:

$$n_{(\mathrm{ACP})} - n_{(\mathrm{BCP})} + n_{(\mathrm{RCP})} - n_{(\mathrm{CCP})} = 1 \tag{22}$$

The eigenvalues of Hessian matrix, λ_1 and λ_2, are negative and $|\lambda_1| < |\lambda_2|$ for the BCP. λ_1 and λ_2 are perpendicular to the bonding path, and λ_3 is a positive value along the bonding path. For the QTAIM analysis, it is necessary to know the electron density $\rho(r)$ and Laplacian electron density $\nabla^2 \rho(r)$. The $\rho(r)$ and $\nabla^2\rho(r)$ play an important role in the segmentation and identification of different types of chemical interactions. A BCP with negative values of $\nabla^2\rho(r)$ and large values of $\rho(r)$ (of orders exceeding 10–1 a.u.) is defined as a shared (covalent) intermolecular interaction. Also, when $\nabla^2\rho(r)$ is positive, the interactions can be classified as of the non-substrate close-shell type (which include ionic and van der Waals interactions) [97]. The elliptical bond (ε) [98] and the virial theorem [99] are two other important factors in the classification of bonds. An elliptical bond represents the electron density preferentially accumulated on a plate containing the bond and is defined as follows:

$$\varepsilon = \frac{\lambda_1}{\lambda_2} - 1 \text{ where } |\lambda_1| > |\lambda_2| \tag{23}$$

Large values of ε indicate an unstable structure and vice versa. Also, based on the virial theorem, the following relationship exists between the electron kinetic energy density $G(r)$ [100], the electron potential energy density $V(r)$ [101], and $\nabla^2\rho(r)$:

$$\frac{1}{4}\nabla^2\rho(r) = 2G(r) + V(r) \tag{24}$$

The balance between $G(r)$ and $V(r)$ reflects the nature of the interaction, and therefore, the ratio of $G/|V|$ can be used as an appropriate index in link classification. If this ratio is less than 0.5, the nature of the interaction will be purely covalent, and if the ratio is greater than 1, the interaction may be considered as completely non-covalent. Note that for covalent bonds (i.e., $\nabla^2\rho(r) < 0$ and $G/|V| < 0.5$), the nature of the bond changes from van der Waals interactions to strong covalent interactions. It becomes covalent. It can also play a decisive role in controlling the amount of ionic interaction for close-shell interactions (i.e., $\nabla^2\rho(r) > 0$ and $G/|V| > 1$), as they become stronger ionically (and weakly electrostatic) by reducing

Table 7 The AIM topological parameters, including electron density ($\rho(r)$), Laplacian of electron density ($\nabla^2\rho(r)$), the kinetic electron density $G(r)$, potential electron density $V(r)$, eigenvalues of Hessian matrix (λ), and bond ellipticity index (ε) at BCP of the BCF clusters with SiCNT and SiCGeNT. All values have been calculated using the PBEPBE/6-311G(d) level of theory from NBO analysis

Systems	Bond	ρ	$\nabla^2 r$	$G(r)$	$V(r)$	$G(r)/V(r)$	λ_1	λ_2	λ_3	ε
$CBrClF_2$	C—Br	0.1493	− 0.1266	0.0552	− 0.1421	0.3886	− 0.1898	0.2564	− 0.1931	0.0172
	C—Cl	0.1895	− 0.2221	0.0651	− 0.1858	0.3505	− 0.2986	0.3836	− 0.3071	0.0286
	C—F	0.2808	− 0.2899	0.3422	− 0.7569	0.4521	− 0.5630	0.8794	− 0.6064	0.0771
SiCNT	Si—C	0.1230	0.3720	0.1620	− 0.231	0.7010	− 0.168	0.6790	− 0.139	0.2110
SiCGeNT	Si—C	0.1233	0.3721	0.1620	− 0.2309	0.7014	− 0.1682	0.6791	− 0.1388	0.2121
	Ge—C	0.1391	0.1714	0.1250	− 0.2072	0.6034	− 0.1495	0.4817	− 0.1607	0.0748
$CBrClF_2$/SiCNT	Br....C	0.0041	0.0161	0.0032	− 0.0024	1.3492	− 0.0026	0.0207	− 0.0020	0.3089
	Br....Si	0.0165	0.0288	0.0073	− 0.0075	0.9806	− 0.0091	0.0450	− 0.0071	0.2734
	Cl....Si	0.0028	0.0075	0.0014	− 0.0009	1.5279	− 0.0013	0.0094	− 0.0006	1.2996
	C—Br	0.1442	− 0.1163	0.0517	− 0.1324	0.3902	− 0.1847	0.2569	− 0.1885	0.0207
	C—Cl	0.1918	− 0.2283	0.0663	− 0.1896	0.3495	− 0.3113	0.3852	− 0.3021	0.0302
	C—F	0.2817	− 0.2804	0.3468	− 0.7636	0.4541	− 0.5655	0.8945	− 0.6095	0.0779
$CBrClF_2$/SiCGeNT	Br....Si	0.0052	0.0202	0.0041	− 0.0030	1.3304	− 0.0035	0.0260	− 0.0023	0.5597
	Br....Ge	0.0266	0.0501	0.0141	− 0.0156	0.9011	− 0.0158	0.0831	− 0.0172	0.0874
	F....Si	0.0043	0.0155	0.0030	− 0.0022	1.3895	− 0.0027	0.0199	− 0.0018	0.5131
	C—Br	0.1434	− 0.1128	0.0516	− 0.1314	0.3927	− 0.1845	0.2577	− 0.1861	0.0087
	C—Cl	0.1927	− 0.2322	0.0667	− 0.1915	0.3484	− 0.3031	0.3836	− 0.3127	0.0317
	C—F	0.2777	− 0.3026	0.3321	− 0.7398	0.4489	− 0.5500	0.8407	− 0.5932	0.0785

interactions. Therefore, the QTAIM topology analysis together with WBI analysis and adsorption results exposes an important trend: by increasing the ionic character of atomic bonds in the nanotubes, the tendencies of the gases to adsorb are also increased.

Considerable results can be obtained from reviewing Table 7. It is observed that in all adsorption sites, Laplacian of electron energy density has a positive value; i.e., the bond is non-covalent. In the study of doped systems, we found that for the all clusters, the energy density and the energy density of Laplacian are high indicating that there is a strong bond between the nanotubes and the BCF molecule, and the elliptical bond is close to 0, which means that the interaction is strong. As stated above, the ratio $G/|V|$ more than 1 means non-covalent bonding; in the case of Ge-doped clusters, these amounts are less than 1. In other words, the results of QTAIM analysis also confirm the strong adsorption of the BCF molecule on the SiCGeNT which is illustrated in Fig. 6.

The reduced density gradient (RDG) function as well as $\mathrm{sign}\lambda_2(r)\rho(r)$ is used to evaluate the weak interactions. These functions are categorized in the context of non-covalent interaction methods which is a powerful way to analyze the types of intermolecular interactions. The RGD is defined as follows [102, 103]:

$$\mathrm{RDGs} = \frac{1}{2(3\pi^2)^{\frac{1}{3}}\overline{\rho((r))}^{\frac{4}{3}}} \tag{25}$$

The strength of the interaction has a positive correlation with electron density ρ(r) and the second largest eigenvalue of the Hessian matrix (λ_2). Thus, the real space function $\mathrm{sign}\lambda_2(r)\rho(r)$ (the products of the signs of λ_2 and ρ) can be defined. The scatter graph of the sign of the $\lambda_2(r)\rho(r)$ function (*X*-axis) and RDG (*Y*-axis) reveals the interaction type between gases and nanotubes. The RDG values range from medium to very large around the nuclei and edges of the molecules, whereas weak interactions (zero to medium) are observed around the chemical bonds. Also, for each specific value of RDG (seen as a horizontal line on the graph), the regions of the graph can be classified into three types, namely, $\mathrm{sign}\lambda_2(r)\rho(r) < 0$ (strong attraction), $\mathrm{sign}\lambda_2(r)\rho(r) \approx 0$ (weak van der Waals interaction), and $\mathrm{sign}\lambda_2(r)\rho(r) > 0$ (strong repulsion (steric effect in ring)) [102, 103].

Using the isosurface RDG = 0.5 as a reference, it can be concluded that after adsorption of the gas onto the outer surfaces of the nanotubes, spots appeared around the region characterized by $\mathrm{sign}\lambda_2(r)\rho(r) \approx 0$. The interaction of gas with SiC nanotubes is in the range of strong van der Waals interactions in nature. Significant changes in the overall features of the pristine nanotube graph (Fig. 7) after the adsorption of gases were observed in the region characterized as $\mathrm{sign}\lambda_2(r)\rho(r) < 0$ (i.e., strong attraction), implying that the nanotube/gas interactions were strong. Hence, this analysis also confirms the results of

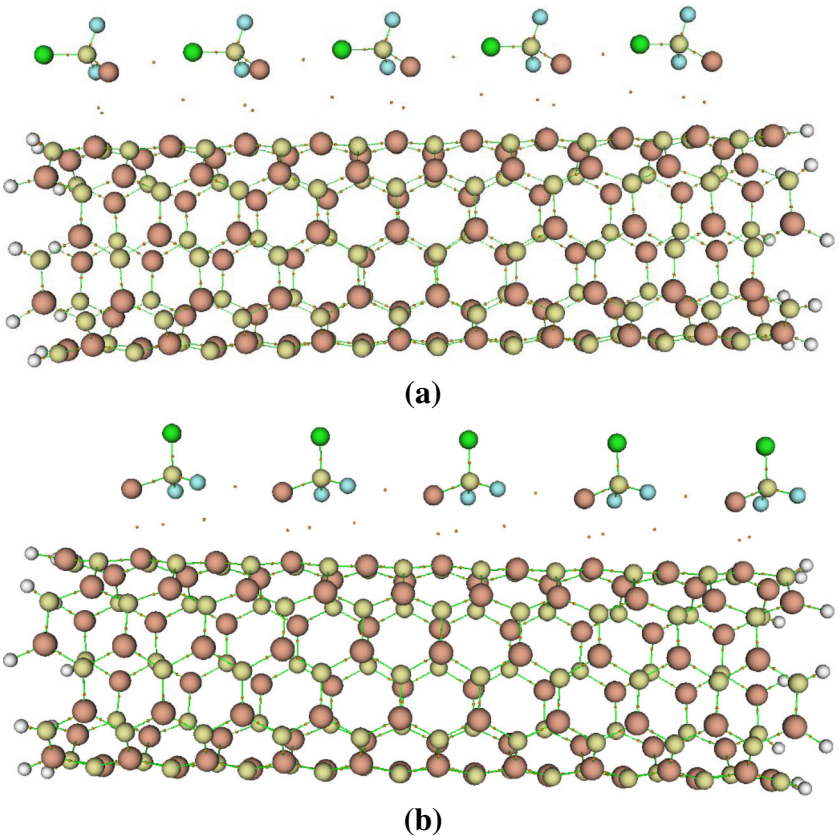

Fig. 6 AIM molecular graphs for (**a**) BCF/SiCNT and (**b**) BCF/SiCGeNT systems. Orange dots represent the boundary critical points (BCP)

the single-point energy calculations and NBO analysis, namely, that the interactions of BCF with SiCNT and SiCGeNT were strong.

Conclusion

In this study, the interactions between bromochlorodifluoromethane molecule and pristine and Ge-

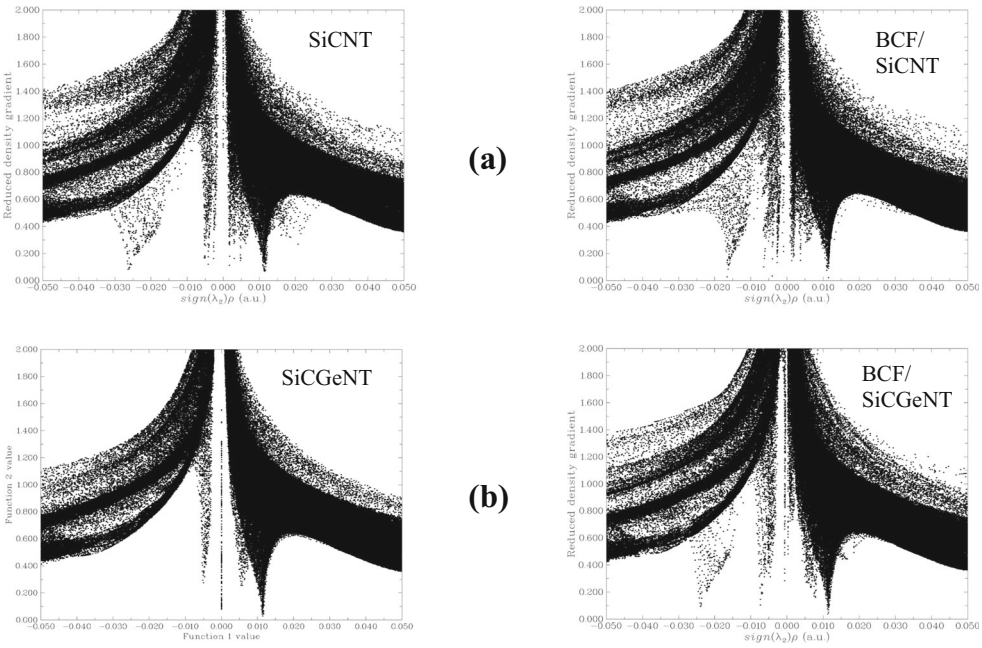

Fig. 7 Plots for the reduced density gradient (RDG) vs. sign(λ_2)ρ(r) values of the (**a**) pristine and (**b**) Ge-doped silicon carbide nanotubes. The data were obtained from completed nanotube and PBEPBE/6-311G (d) level of theory. The left side diagrams are isolated nanotubes and the right side diagrams are BCF/nanotube clusters

doped silicon carbide nanotubes were investigated using density functional theory framework. To this end, the structure of the nanotubes and BCF molecule was optimized using PBC-DFT method at the theoretical level of PBEPBE/6-311G (d). Right after optimization calculation, the B3LYP, CAM-B3LYP, M06-2X, and ωB97XD functionals and same basis set were also used to consider the contribution of long-range interactions and dispersion effect for single-point energy calculation. QTAIM and NBO analyses were also implemented to consider the character of intermolecular interactions. The results of all analyses are in agreement and show that (1) among the different positions studied for pristine silicon carbide nanotube, the T_2 position has the highest absorption energy; (2) by inserting germanium as an impurity in silicon carbide nanotube, the symmetrical structure of the nanotubes is changed and the electronic properties and consequently the chemical properties of the nanotubes are changed accordingly; (3) the Ge-doped SiCNT has a very high adsorption energy compared with SiCNT, and is expected to be strong physical adsorption in this case and appears to be a suitable sensor characteristic option. Finally, we conclude that between the studied absorbent, the SiCGeNT is a more favorable candidate for utilization as gas sensor devices to detect the BCF molecule.

Acknowledgments I would like to thank the Solid-State Theory Group at the Physics Department at the Universita'degli Studi di Milano-Italy for providing computational facilities.

Compliance with ethical standards

Conflict of interest The authors declare that they have no conflict of interest.

References

1. Iijima S, Ichihashi T (1993) Single-shell carbon nanotubes of 1-nm diameter. Nature 363:603–605
2. Bethune D, Kiang CH, De Vries M, Gorman G, Savoy R, Vazquez J, Beyers R (1993) Cobalt-catalysed growth of carbon nanotubes with single-atomic-layer walls. Nature 363:605–607
3. Monthioux M, Kuznetsov VL (2006) Who should be given the credit for the discovery of carbon nanotubes? Carbon 44:1621–1623
4. Eklund P, Ajayan P, Blackmon R, Hart AJ, Kibng J, Pradhan B, Bao A, Rinzler A (2007) International assessment of research and development of carbon nanotube manufacturing and applications
5. Iijima S (1991) Helical microtubules of graphitic carbon. Nature 354:56–58
6. Mintmire JW, Dunlap BI, White CT (1992) Are fullerene tubules metallic? Phys Rev Lett 68:631
7. Pujadó MP (2012) Carbon nanotubes as platforms for biosensors with electrochemical and electronic transduction, Springer Science & Business Media
8. Filleter T, Bernal R, Li S, Espinosa HD (2011) Ultrahigh strength and stiffness in cross-linked hierarchical carbon nanotube bundles. Adv Mater 23:2855–2860
9. Peng B, Locascio M, Zapol P, Li S, Mielke SL, Schatz GC, Espinosa HD (2008) Measurements of near-ultimate strength for multiwalled carbon nanotubes and irradiation-induced crosslinking improvements. Nat Nanotechnol 3:626
10. Yu M-F, Lourie O, Dyer MJ, Moloni K, Kelly TF, Ruoff RS (2000) Strength and breaking mechanism of multiwalled carbon nanotubes under tensile load. Science 287:637–640
11. Makarova T, Palacio F (2006) Carbon based magnetism: an overview of the magnetism of metal free carbon-based compounds and materials, Elsevier
12. Tang Z, Zhang L, Wang N, Zhang X, Wen G, Li G, Wang J, Chan CT, Sheng P (2001) Superconductivity in 4 angstrom single-walled carbon nanotubes. Science 292:2462–2465
13. Tans SJ, Devoret MH, Dai H, Thess A, Smalley RE, Geerligs L, Dekker C (1997) Individual single-wall carbon nanotubes as quantum wires. Nature 386:474–477
14. Vasylenko A, Wynn J, Medeiros PV, Morris AJ, Sloan J, Quigley D (2017) Encapsulated nanowires: boosting electronic transport in carbon nanotubes. Phys Rev B 95:121408
15. Zhang R, Zhang Y, Zhang Q, Xie H, Qian W, Wei F (2013) Growth of half-meter long carbon nanotubes based on Schulz–Flory distribution. ACS Nano 7:6156–6161
16. Berber S, Kwon Y-K, Tománek D (2000) Unusually high thermal conductivity of carbon nanotubes. Phys Rev Lett 84:4613
17. Karousis N, Tagmatarchis N, Tasis D (2010) Current progress on the chemical modification of carbon nanotubes. Chem Rev 110:5366–5397
18. Mingo N, Stewart DA, Broido DA, Srivastava D (2008) Phonon transmission through defects in carbon nanotubes from first principles. Phys Rev B 77:033418
19. Pop E, Mann D, Wang Q, Goodson K, Dai H (2006) Thermal conductance of an individual single-wall carbon nanotube above room temperature. Nano Lett 6:96–100
20. Nalwa HS (2004) Encyclopedia of Nanoscience and Nanotechnology; Volume 10, American scientific publishers
21. S. Choudhary, Spin transport in H2O adsorbed SiCNT based magnetic tunnel junction using half metallic ferromagnetic electrodes, Advanced Science, Engineering and Medicine, 9 (2017) 943–947
22. Choudhary S, Qureshi S (2011) Theoretical study on transport properties of a BN co-doped SiC nanotube. Phys Lett A 375:3382–3385
23. Mpourmpakis G, Froudakis GE, Lithoxoos GP, Samios J (2006) SiC nanotubes: a novel material for hydrogen storage. Nano Lett 6:1581–1583
24. Wang X, Liew KM (2011) Hydrogen storage in silicon carbide nanotubes by lithium doping. J Phys Chem C 115:3491–3496
25. Cao F, Sun H (2012) Theoretical study on the possibility of using silicon carbide nanotubes as dehydrogenation catalysts for ammonia–borane. RSC Adv 2:7561–7568
26. Ganji M, Ahaz B (2010) First principles simulation of molecular oxygen adsorption on SiC nanotubes. Commun Theor Phys 53:742
27. Mercan K, Civalek Ö (2016) Buckling analysis of silicon carbide nanotubes (SiCNTs). International Journal of Engineering and Applied Sciences 8:101–108
28. Mohammadi MD, Hamzehloo M (2018) The adsorption of bromomethane onto the exterior surface of aluminum nitride, boron nitride, carbon, and silicon carbide nanotubes: a PBC-DFT, NBO, and QTAIM study. Computational and Theoretical Chemistry 1144:26–37
29. Nemati-Kande E, Abbasi M, Doust Mohammadi M (2018) DFT, QTAIM and NBO investigation of the interaction of rare gases with pristine and decorated boron nitride nanotube. ChemistrySelect 3:9833–9840
30. Nemati-Kande E, Abbasi M, Mohammadi MD (2020) DFT studies on the interactions of pristine, Al and Ga-doped boron nitride

nanosheets with CH3X (X= F, Cl and Br). J Mol Struct 1199: 126962
31. Nemati-Kande E, Abbasi M, Mohammadi MD (2019) Feasibility of pristine and decorated AlN and SiC nanotubes in sensing of noble gases: a DFT study. ChemistrySelect 4:2453–2462
32. Nemati-Kande E, Karimian R, Goodarzi V, Ghazizadeh E (2020) Feasibility of pristine, Al-doped and Ga-doped boron nitride nanotubes for detecting SF4 gas: a DFT, NBO and QTAIM investigation. Appl Surf Sci 510:145490
33. Adhikari K, Ray A (2011) Carbon-and silicon-capped silicon carbide nanotubes: an ab initio study. Phys Lett A 375:1817–1823
34. Mavrandonakis A, Froudakis GE, Schnell M, Mühlhäuser M (2003) From pure carbon to silicon− carbon nanotubes: an ab-initio study. Nano Lett 3:1481–1484
35. Alam KM, Ray AK (2007) A hybrid density functional study of zigzag SiC nanotubes. Nanotechnology 18:495706
36. Zhang Y, Huang H (2008) Stability of single-wall silicon carbide nanotubes–molecular dynamics simulations. Comput Mater Sci 43:664–669
37. Baei MT, Peyghan AA, Moghimi M, Hashemian S (2012) Effect of gallium doping on electronic and structural properties (6, 0) zigzag silicon carbide nanotube as a p-semiconductor. Journal of Cluster Science 23:1119–1132
38. Gao K, Chen G, Wu D (2014) A DFT study on the interaction between glycine molecules/radicals and the (8, 0) SiCNT. Phys Chem Chem Phys 16:17988–17997
39. Javan MB (2015) Adsorption of CO and NO molecules on SiC nanotubes and nanocages: DFT study. Surf Sci 635:128–142
40. Gao G, Kang HS (2008) First principles study of NO and NNO chemisorption on silicon carbide nanotubes and other nanotubes. J Chem Theory Comput 4:1690–1697
41. Nematollahi P, Esrafili MD (2016) A DFT study on the N 2 O reduction by CO molecule over silicon carbide nanotubes and nanosheets. RSC Adv 6:59091–59099
42. Mahdavifar Z, Abbasi N, Shakerzadeh E (2013) A comparative theoretical study of CO2 sensing using inorganic AlN, BN and SiC single walled nanotubes. Sensors and Actuators B: Chemical 185:512–522
43. Binbrek OS, Torrie BH, Swainson IP (2002) Neutron powder-profile study of chlorofluoromethane. Acta Crystallogr Sect C: Cryst Struct Commun 58:o672–o674
44. U.N.E.P.O. Secretariat, Handbook for the Montreal protocol on substances that deplete the ozone layer, UNEP/Earthprint2006
45. Favero LB, Maris A, Melandri S, Ottaviani P, Caminati W (2019) Non covalent interactions stabilizing the chiral dimer of CH 2 ClF: a rotational study. Phys Chem Chem Phys 21:3695–3700
46. Perdew JP, Burke K, Ernzerhof M (1996) Generalized gradient approximation made simple. Phys Rev Lett 77:3865
47. Hehre WJ, Ditchfield R, Pople JA (1972) Self—consistent molecular orbital methods. XII. Further extensions of Gaussian—type basis sets for use in molecular orbital studies of organic molecules. J Chem Phys 56:2257–2261
48. Frisch MJ, Trucks GW, Schlegel HB, Scuseria GE, Robb MA, Cheeseman JR, Scalmani G, Barone V, Petersson GA, Nakatsuji H, Li X, Caricato M, Marenich AV, Bloino J, Janesko BG, Gomperts R, Mennucci B, Hratchian HP, Ortiz JV, Izmaylov AF, Sonnenberg JL, Ding WF, Lipparini F, Egidi F, Goings J, Peng B, Petrone A, Henderson T, Ranasinghe D, Zakrzewski VG, Gao J, Rega N, Zheng G, Liang W, Hada M, Ehara M, Toyota K, Fukuda R, Hasegawa J, Ishida M, Nakajima T, Honda Y, Kitao O, Nakai H, Vreven T, Throssell K, Montgomery JA Jr., Peralta JE, Ogliaro F, Bearpark MJ, Heyd JJ, Brothers EN, Kudin KN, Staroverov VN, Keith TA, Kobayashi R, Normand J, Raghavachari K, Rendell AP, Burant JC, Iyengar SS, Tomasi J, Cossi M, Millam JM, Klene M, Adamo C, Cammi R, Ochterski JW, Martin RL, Morokuma K, Farkas O, Foresman JB, Fox DJ (2016) Gaussian 16 Rev. C.01, Wallingford, CT
49. Lu T, Chen F (2012) Multiwfn: a multifunctional wavefunction analyzer. J Comput Chem 33:580–592
50. Lu T, Chen F (2012) Quantitative analysis of molecular surface based on improved Marching Tetrahedra algorithm. J Mol Graph Model 38:314–323
51. Lu T, Chen Q (2020) A simple method of identifying π orbitals for non-planar systems and a protocol of studying π electronic structure. Theor Chem Accounts 139:25
52. Becke AD (2014) Perspective: fifty years of density-functional theory in chemical physics. The Journal of chemical physics 140:18A301
53. Bloch F (1929) Über die quantenmechanik der elektronen in kristallgittern. Z Phys 52:555–600
54. Hoffmann R (1987) How chemistry and physics meet in the solid state. Angew Chem Int Ed Engl 26:846–878
55. Kittel C, McEuen P, McEuen P (1996) Introduction to solid state physics, Wiley New York
56. J.B. Foresman, A. Frisch (1996), Exploring chemistry with electronic structure methods: a guide to using Gaussian
57. Parr RG, Donnelly RA, Levy M, Palke WE (1978) Electronegativity: the density functional viewpoint. J Chem Phys 68:3801–3807
58. von Szentpály L (1998) Valence states in molecules. 3. Transferable vibrational force constants from homonuclear data. J Phys Chem A 102:10912–10915
59. Janak J (1978) Proof that∂ e∂ n i= ε in density-functional theory. Phys Rev B 18:7165
60. Parr RG (1980) Density functional theory of atoms and molecules, Horizons of Quantum Chemistry, Springer, pp. 5–15
61. Chattaraj P, Roy D (2007) Perennial review: update 1 of Chem. Rev. 106, 2065 (2006), Chem. Rev, 107
62. R.G. Parr, L.v. Szentpaly, S. Liu, Electrophilicity index, J Am Chem Soc, 121 (1999) 1922-1924
63. Noorizadeh S, Maihami H (2006) A theoretical study on the regioselectivity of Diels–Alder reactions using electrophilicity index. J Mol Struct THEOCHEM 763:133–144
64. Weinhold F (2012), Discovering chemistry with natural bond orbitals, John Wiley & Sons
65. Weinhold F, Landis CR (2005) Valency and bonding: a natural bond orbital donor-acceptor perspective, Cambridge University Press
66. Carpenter J, Weinhold F (1988) Analysis of the geometry of the hydroxymethyl radical by the "different hybrids for different spins" natural bond orbital procedure. J Mol Struct THEOCHEM 169:41–62
67. Foster AJ, Weinhold F (1980) Natural hybrid orbitals. Journal of the American Chemical Society 102:7211–7218
68. Glendening E, Badenhoop J, Reed A, Carpenter J, Bohmann J, Morales C, Landis C, Weinhold F (2013) NBO 6.0, Theoretical Chemistry Institute, University of Wisconsin, Madison
69. Reed AE, Weinhold F (1983) Natural bond orbital analysis of near-Hartree–Fock water dimer. J Chem Phys 78:4066–4073
70. Reed AE, Weinhold F (1985) Natural localized molecular orbitals. J Chem Phys 83:1736–1740
71. Reed AE, Weinstock RB, Weinhold F (1985) Natural population analysis. J Chem Phys 83:735–746
72. Glendening ED, Landis CR, Weinhold F (2012) Natural bond orbital methods. Wiley interdisciplinary reviews: computational molecular science 2:1–42
73. Glendening ED, Landis CR, Weinhold F (2019) NBO 7.0: new vistas in localized and delocalized chemical bonding theory. J Comput Chem 40:2234–2241

74. Reed AE, Curtiss LA, Weinhold F (1988) Intermolecular interactions from a natural bond orbital, donor-acceptor viewpoint. Chem Rev 88:899–926
75. Weinhold F (2002) Natural bond orbital methods, Encyclopedia of computational chemistry, 3
76. Weinhold F (2012) Natural bond orbital analysis: a critical overview of relationships to alternative bonding perspectives. J Comput Chem 33:2363–2379
77. Weinhold F, Landis C, Glendening E (2016) What is NBO analysis and how is it useful? Int Rev Phys Chem 35:399–440
78. Mulliken RS (1955) Electronic population analysis on LCAO–MO molecular wave functions. I. J Chem Phys 23:1833–1840
79. Mayer I (1983) Charge, bond order and valence in the AB initio SCF theory. Chem Phys Lett 97:270–274
80. Mayer I (2012) Improved definition of bond orders for correlated wave functions. Chem Phys Lett 544:83–86
81. Giambiagi M, de Giambiagi MS, Mundim KC (1990) Definition of a multicenter bond index. Struct Chem 1:423–427
82. Matito E (2016) An electronic aromaticity index for large rings. Phys Chem Chem Phys 18:11839–11846
83. Wiberg KB (1968) Application of the pople-santry-segal CNDO method to the cyclopropylcarbinyl and cyclobutyl cation and to bicyclobutane. Tetrahedron 24:1083–1096
84. Lu T, Chen F (2013) Bond order analysis based on the Laplacian of electron density in fuzzy overlap space. J Phys Chem A 117: 3100–3108
85. Mayer I, Salvador P (2004) Overlap populations, bond orders and valences for 'fuzzy'atoms. Chem Phys Lett 383:368–375
86. Sizova OV, Skripnikov LV, Sokolov AY (2008) Symmetry decomposition of quantum chemical bond orders. J Mol Struct THEOCHEM 870:1–9
87. Bader R, Nguyen-Dang TT, Tal Y (1981) A topological theory of molecular structure. Rep Prog Phys 44:893
88. Bader RF (1985) Atoms in molecules. Acc Chem Res 18:9–15
89. Bader RF (1991) A quantum theory of molecular structure and its applications. Chem Rev 91:893–928
90. Bader RF, Matta CF (2013) Atoms in molecules as non-overlapping, bounded, space-filling open quantum systems. Found Chem 15:253–276
91. Biegler-könig FW, Bader RF, Tang TH (1982) Calculation of the average properties of atoms in molecules. II. J Comput Chem 3: 317–328
92. Cortés-Guzmán F, Bader RF (2005) Complementarity of QTAIM and MO theory in the study of bonding in donor–acceptor complexes. Coord Chem Rev 249:633–662
93. Howard S, Krygowski T (1997) Benzenoid hydrocarbon aromaticity in terms of charge density descriptors. Can J Chem 75:1174–1181
94. Noorizadeh S, Shakerzadeh E (2010) Shannon entropy as a new measure of aromaticity, Shannon aromaticity. Physical Chemistry Chemical Physics 12:4742–4749
95. Balanarayan P, Gadre SR (2003) Topography of molecular scalar fields. I. Algorithm and Poincaré–Hopf relation. J Chem Phys 119:5037–5043
96. Roy D, Balanarayan P, Gadre SR (2008) An appraisal of Poincaré–Hopf relation and application to topography of molecular electrostatic potentials. J Chem Phys 129:174103
97. Matta CF (2006) Hydrogen–hydrogen bonding: the non-electrostatic limit of closed-shell interaction between two hydro, hydrogen bonding—new insights, Springer, pp. 337–375
98. Bohórquez HJ, Boyd RJ, Matta CF (2011) Molecular model with quantum mechanical bonding information. J Phys Chem A 115: 12991–12997
99. Grabowski SJ (2012) QTAIM characteristics of halogen bond and related interactions. J Phys Chem A 116:1838–1845
100. Tal Y, Bader R (1978) Studies of the energy density functional approach. I. Kinetic energy. Int J Quantum Chem 14:153–168
101. Keith T, Bader R, Aray Y (1996) Structural homeomorphism between the electron density and the virial field. Int J Quantum Chem 57:183–198
102. Contreras-García J, Johnson ER, Keinan S, Chaudret R, Piquemal J-P, Beratan DN, Yang W (2011) NCIPLOT: a program for plotting noncovalent interaction regions. J Chem Theory Comput 7: 625–632
103. Johnson ER, Keinan S, Mori-Sánchez P, Contreras-García J, Cohen AJ, Yang W (2010) Revealing noncovalent interactions. J Am Chem Soc 132:6498–6506